Journal of Materials Science & Technology 33 (2017) 1009–1014

Contents lists available at ScienceDirect

Journal of Materials Science & Technology

journal homepage: www.jmst.org

Enhanced Mechanical Properties of Friction Stir Welded 5083Al-H19 Joints with Additional Water Cooling

B.B. Wang [a], F.F. Chen [b], F. Liu [a], W.G. Wang [a,*], P. Xue [b,*], Z.Y. Ma [b]

[a] School of Mechanical Engineering, Liaoning Shihua University, Fushun 113001, China
[b] Shenyang National Laboratory for Materials Science, Institute of Metal Research, Chinese Academy of Sciences, Shenyang 110016, China

ARTICLE INFO

Article history:
Received in revised form 28 October 2016
Accepted 22 November 2016
Available online 8 January 2017

Keywords:
Friction stir welding
Aluminum alloy
Water cooling
Microstructure
Mechanical property

ABSTRACT

3-mm-thick 5083Al-H19 rolled plates were friction stir welded (FSW) at tool rotation rates of 800 and 200 rpm with and without additional water cooling. With decreasing the rotation rate and applying water cooling, softening in the FSW joint was significantly reduced. At a low rotation rate of 200 rpm with additional water cooling, almost no obvious softening was observed in the FSW joint, and therefore a FSW 5083Al-H19 joint with nearly equal strength to the base material (BM) was obtained. Furthermore, the grains in the nugget zone were considerably refined with reducing the heat input and ultrafine equiaxed grains of about 800 nm were obtained in the lowest heat input condition. This work provides an effective method to achieve high property FSW joints of precipitate-hardened and work-hardened Al alloys.

1. Introduction

5xxx series Al alloy is one of the most widely used alloys in the fields of aerospace and automobile due to its good corrosion resistance, good weldability and high specific strength. During the industrial applications, welding is an indispensable and important process for structure manufacturing. In the fusion welding method, poor solidification microstructure with crack and porosity may be achieved in the fusion zone, leading to a significant loss in mechanical properties compared to the base material (BM). Further, serious softening is a common phenomenon due to the large heat input during the fusion welding, especially for the initial work-hardened BM with an H state.

Friction stir welding (FSW) as a solid-state joining process exhibits various advantages compared to the conventional fusion welding techniques, such as energy efficiency, environmental friendliness, and versatility [1]. FSW has been successfully used in various industries which involved Al alloys, such as aerospace, marine, and rail transit. However, FSW still creates a softened region in the joints of work-hardened and precipitate-hardened Al alloys by using the normal parameters. Such softening is caused by the decrease of dislocation density and the dissolution and coarsening of strengthening precipitates during the thermal cycle of FSW [1–3].

Usually, the joint coefficient was about 60%–70% for the normal FSW joints of the precipitate-hardened Al alloys [4–6]. For the work-hardened 5xxx series Al alloys, though a relatively high joint coefficient of 97% was achieved in H111 state and 85% in H321 state, the yield strength (YS) only reached 70% of that of the BM [7,8]. Further, the YS and ultimate tensile strength (UTS) of the FSW joints decreased more seriously for 5xxx series Al alloys with more work-hardening amount, such as H34, H38 and H19 state [9].

Obviously, softening in the weld zone, including nugget zone (NZ), thermal mechanical affected zone (TMAZ) and the heat affected zone (HAZ), is an important problem for the FSW joint of the work-hardened and precipitate-hardened Al alloys, which is greatly related to the heat input during welding. Many researchers have concentrated on decreasing the rotation rate and/or increasing the welding speed to reduce the heat input in order to enhance the strength of FSW joints [8]. However, the results indicated that defects were easily formed at very low rotation rate or high welding speed [10–12].

In addition to changing the rotation rate and welding speed, additional cooling is an effective method of reducing the heat input during FSW. Some researchers have performed FSW with various additional cooling mediums, such as water, liquid nitrogen and dry ice [13–20]. Among these methods, FSW with water cooling is a high efficient and low cost welding method, catching more and more attention [15–20]. FSW with additional water cooling has

* Corresponding authors.
E-mail addresses: wgwang@imr.ac.cn (W.G. Wang), pxue@imr.ac.cn (P. Xue).

http://dx.doi.org/10.1016/j.jmst.2017.01.016
1005-0302/

been demonstrated to be an effective method of improving the mechanical properties of FSW Al alloy joints.

Zhang et al. [18] investigated the effect of underwater FSW on the mechanical properties of the 2219Al-T6 joints, and a maximum tensile strength of 360 MPa was achieved which was higher than that of the normal FSW joint. Xue et al. [19] indicated that pure Cu (H state) joints with nearly equal strength to the BM were obtained by FSW with rapid water cooling, which is originated from the significantly reduced softening due to considerable decrease in the peak temperature and the duration time at high temperature.

Though FSW with water cooling has attracted much attention recently, the investigation is still limited compared to the normal FSW, and no related studies on work-hardened 5xxx series Al alloys were performed. Further, greatly enhanced mechanical properties were seldom achieved in FSW joints of work-hardened and precipitate-hardened Al alloys with additional cooling from the previous studies [17,18].

In this work, we chose a typical 5xxx series Al alloy – 5083 Al with H19 state as the target BM, to conduct FSW with additional water cooling. The aim of this study is to achieve high property FSW joints of work-hardened 5083 Al alloy and understand the microstructure evolution during FSW.

2. Experimental Procedures

3-mm-thick 5083Al-H19 rolled plates, which were cold rolled without annealing, were used as the BM. Plates with a length of 300 mm and a width of 70 mm were butt welded along the rolling direction with a tool tilt angle of 3°. using a FSW machine. The plates were mechanically polished to remove the oxide and cleaned with the alcohol before the welding procedure, and the final plate thickness was about 2.8 mm.

Normal FSW was conducted at a constant welding speed of 100 mm/min with different tool rotation rates of 800 and 200 rpm, which were defined as A-800 and A-200, respectively. In order to further reduce the heat input, FSW was performed with the same parameters under additional water cooling, and the FSW joints were defined as W-800 and W-200 for the used rotation rates of 800 and 200 rpm, respectively. The 5083Al plates were first fixed in water and additional rapid cooling with flowing water was performed during the welding procedure. A FSW tool with a concave shoulder 12 mm in diameter and a conical threaded pin 4 mm in diameter and 2.6 mm in length were used.

The specimens for microstructural examinations were cross sectioned perpendicular to the FSW direction. Microstructural characterization and analysis were carried out using optical microscopy (OM), scanning electron microscopy (SEM) equipped with electron backscatter diffraction (EBSD), and transmission electron microscopy (TEM). The specimens for OM observation were ground, polished, and then etched in a solution of 15 ml HF, 45 ml HCl, 12 ml HNO_3, and 128 ml H_2O for about 20–30 s. EBSD specimens were ground and then electro-polished in a solution of 10 ml $HClO_4$ and 90 ml C_2H_5OH at 6 V for 10–15 s. TEM foils were prepared by double-jet electrolytic polishing using a solution of 30 ml HNO_3 and 70 ml CH_3OH at 248 K under a potential of 12 V.

Vickers microhardness measurement was conducted on the cross-section perpendicular to the welding direction under a load of 200 g for a holding time of 15 s. The microhardness profiles were obtained along the mid-thickness of the cross-section of the FSW joints at an interval of 1 mm. The tensile specimens, with a gauge length of 35 mm and a gauge width of 6 mm, were machined perpendicular to the FSW direction. Uniaxial tensile tests were carried out at room temperature at an initial strain rate of $1 \times 10^{-3}\ s^{-1}$.

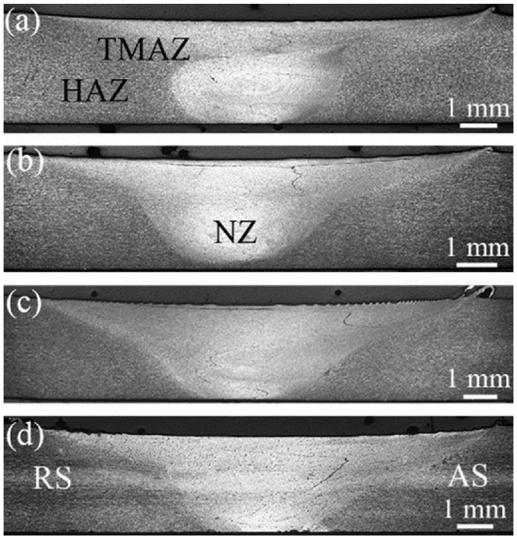

Fig. 1. Cross-sectional macrostructures of various FSW joints: (a) A-800, (b) A-200, (c) W-800, and (d) W-200 samples.

3. Results and Discussion

Fig. 1 shows the cross-sectional macrostructure of the FSW 5083Al-H19 joints. No porosity and tunnel defects were detected in the joints under the four FSW parameters used in this study. Through the macrostructures of the FSW joints, three distinct zones were discernible: the NZ, the TMAZ, and the HAZ. The onion ring structure was only observed in the elliptical NZ of A-800 sample (Fig. 1(a)). When decreasing the rotation rate or applying the additional water cooling, the NZs became basin-shaped without obvious onion ring structure and exhibited larger size than that of A-800 joint. It is well accepted that the heat input was reduced when decreasing the rotation rate and/or using additional water cooling [1,3,19]. Therefore, the viscosity of the material increased in the NZ due to the decreased peak temperature during FSW, and the welding tool would influence more material, so the NZ was enlarged in low heat input condition.

Fig. 2 shows the EBSD microstructures of the NZs for various FSW joints under different parameters. It is clear that equiaxed grains were achieved in the NZs even for the W-200 joint with a very low heat input, which was similar to the microstructural characteristics of the NZs in normal FSW joints and other joints with additional cooling [21–27]. Therefore, the grain refinement mechanism during FSW with water cooling was still dynamic recrystallization (DRX) in this study, and the fine and equiaxed grains were produced in the NZs during DRX process [1,2,28].

From the microstructures in the NZs, it is clear that the grain size decreased with reducing the heat input, and the calculated average grain sizes by EBSD are shown in Table 1. The average grain sizes of A-800 sample and W-800 sample were about 3.6 μm and 2.7 μm, respectively. Clearly, under the relatively high rotation rate of 800 rpm, the grain refinement effect in the NZ was not notable by additional water cooling due to the initial high heat input. Under the air cooling condition, when decreasing the rotation rate to 200 rpm, the grain refinement in the NZ was more notable and the average grain size decreased to 1.8 μm. When further reducing the heat input with the additional water cooling, ultrafine grained structure was achieved in the NZ of the W-200 sample and the average grain size decreased to about 800 nm.

Similar to other DRX structure in the NZs of FSW joints with additional cooling [22,24,26], large fraction of high angle grain boundaries (HAGBs, misorientation angle ≥15°) were obtained in

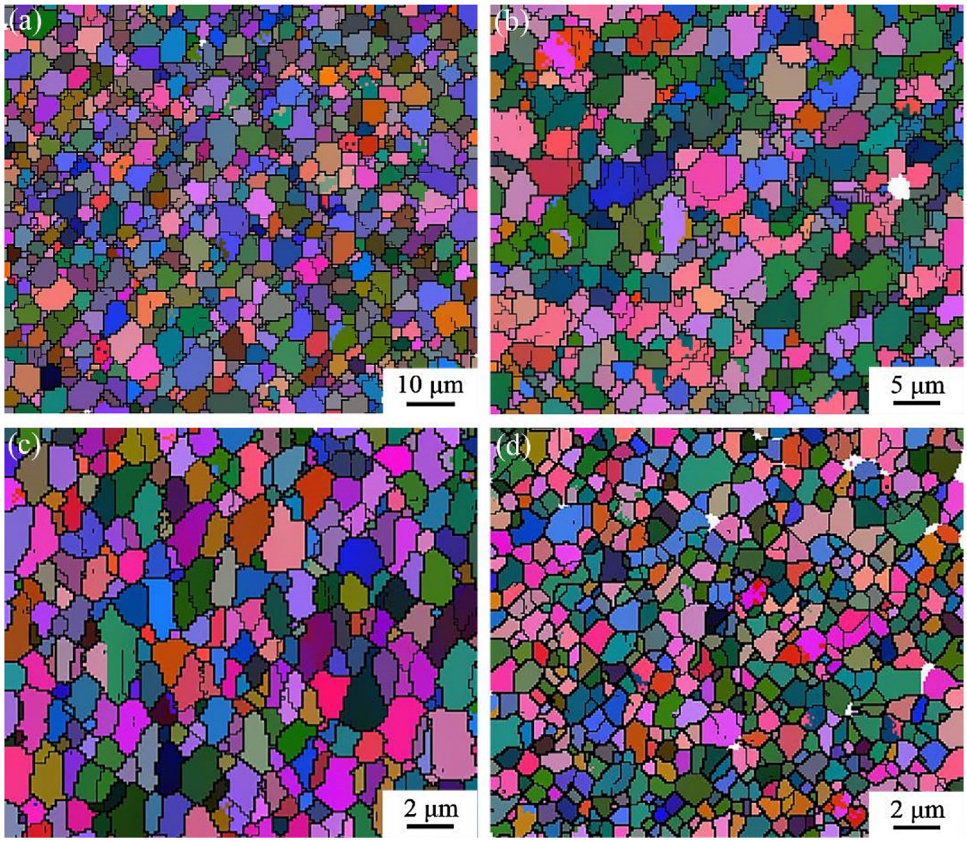

Fig. 2. EBSD microstructures in the NZs of various FSW joints: (a) A-800, (b) W-800, (c) A-200, and (d) W-200 samples.

Table 1
Average grain size in the NZs and mechanical properties of the BM and various FSW joints.

Sample	Grain size in NZ (μm)	Lowest hardness value (HV)	Yield strength (MPa)	Ultimate tensile strength (MPa)	Elongation (%)
BM	–	127	370	425	5.7
A-800	3.6	85	150	314	9.2
A-200	1.8	95	260	344	4.8
W-800	2.7	90	201	328	8.4
W-200	0.8	116	340	403	3.5

the NZs, as shown in Fig. 3. It is noted that the distributions of grain boundary misorientation angles of all FSW samples were similar to the random distribution for a cubic polycrystalline. High fractions of HAGBs (>80%) were obtained in all the samples, and the fractions of the HAGBs reached about 88% in the NZs of normal FSW samples, which should be attributed to the more sufficient DRX structures under slower cooling rate compared to that in water cooling.

The microstructural characteristics of the NZs were further confirmed by the TEM, as shown in Fig. 4. The BM exhibited a typical heavily cold-worked characteristic, and the grains were elongated clearly with the layer width of only about 300 nm (Fig. 4(a)). Meanwhile, very high density of dislocations was observed in the severely deformed grains. Compared to the BM, the dislocation density was significantly reduced in various NZs of the FSW joints, which was consistent with the DRX microstructure. It is clear that the grains in the NZs were equiaxed and most grain boundaries were sharp and relatively straight with clear contrasts between neighboring grains. These characteristics indicated that most of the grain boundaries were HAGBs, which was consistent with the results obtained by EBSD.

From Fig. 4(b), equiaxed fine grains of several micrometers were observed in the NZ of A-800 sample, and many precipitate particles were observed in the grains. 5083 alloy is a solution strengthened Al alloy with high Mg content. During the welding process, the β phase (Al_3Mg_2) will precipitate from the matrix in a temperature between 175–250 °C [29–32]. It is reported that the peak temperature could reach above 450 °C in the NZ during the normal FSW of Al alloys [33,34]. Therefore, β phase particles precipitated from the matrix in the A-800 sample due to the high peak temperature and the severe plastic deformation. As a solution-strengthened alloy, the formation of the precipitate particles will lead to the strength loss of 5xxx series Al alloys. Meanwhile, the high density of dislocations was mostly eliminated due to the strong annealing effect during the FSW thermal cycle.

Similar TEM microstructures were obtained in the W-800 and A-200 samples, and the typical TEM morphology of the A-200 sample is shown in Fig. 4(c). With decreasing the rotation rate to 200 rpm or applying additional water cooling, lower peak temperature and shorter duration at high temperature were achieved, leading to reducing grain size with less precipitate particles. Under a combination of very low rotation rate of 200 rpm and rapid water cooling, the average grain size was greatly reduced in the W-200 sample, and few precipitate particles were observed (Fig. 4(d)). Moreover, it is noted that the dislocation density increased in the NZs of A-200 and W-200 samples compared to the A-800 sample, and many sub-grains and dislocation cells were observed (Fig. 4(c and d)).

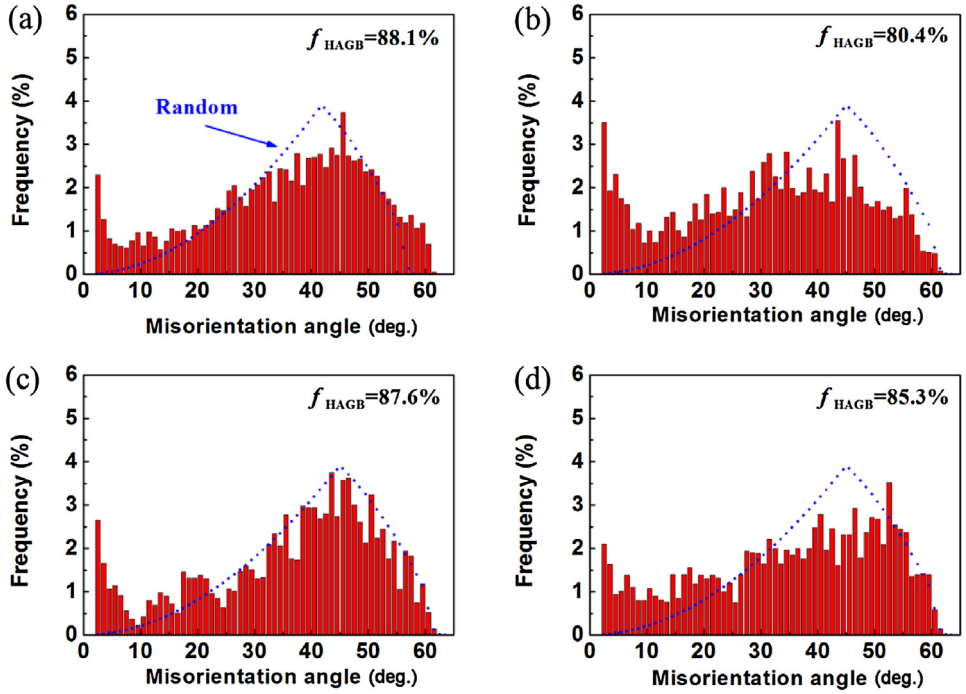

Fig. 3. Distributions of grain boundary misorientation angles in the NZs of various FSW joints: (a) A-800, (b) W-800, (c) A-200, and (d) W-200 samples.

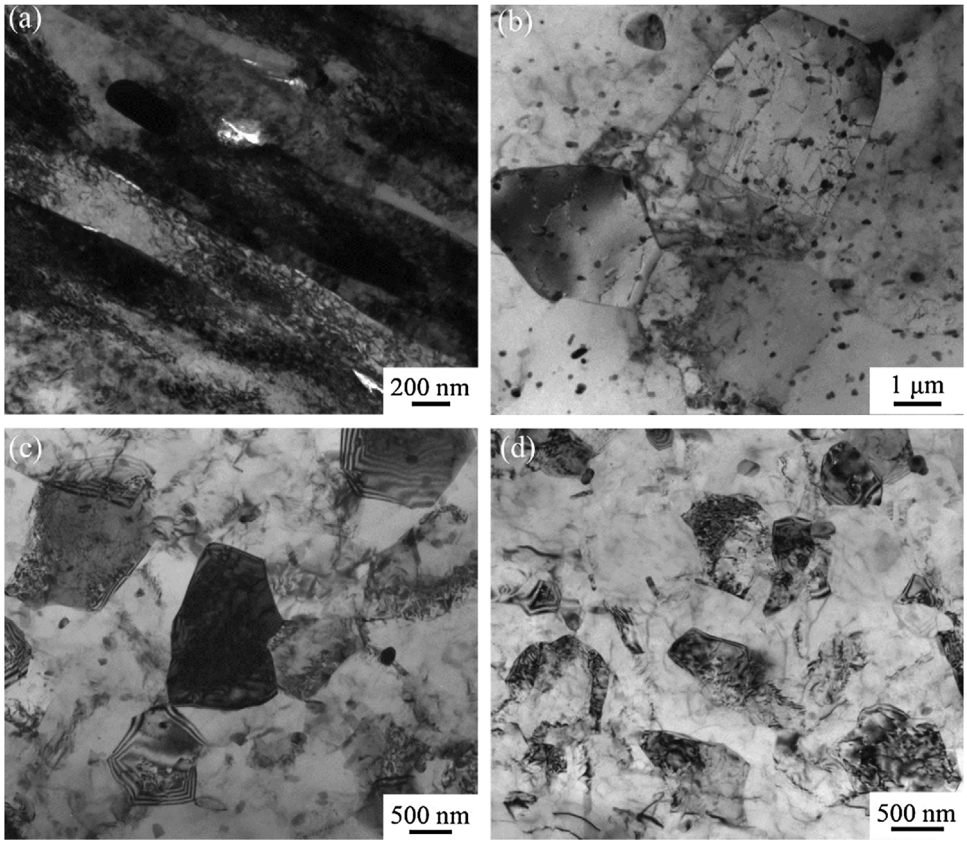

Fig. 4. TEM microstructures of (a) BM, and NZs of FSW joints: (b) A-800, (c) A-200, and (d) W-200 samples.

This should be attributed to the initial high dislocation density in the BM and the reduced heat input under additional water cooling or low rotation rate of 200 rpm.

Fig. 5 depicts the microhardness profiles of the FSW joints under various parameters. The BM exhibited very high hardness value of about 127 HV due to strong work-hardening resulting from cold

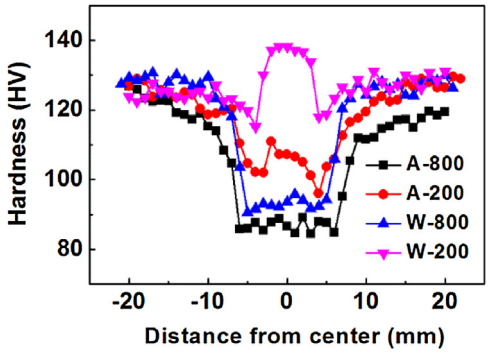

Fig. 5. Microhardness profiles of the FSW joints under various parameters.

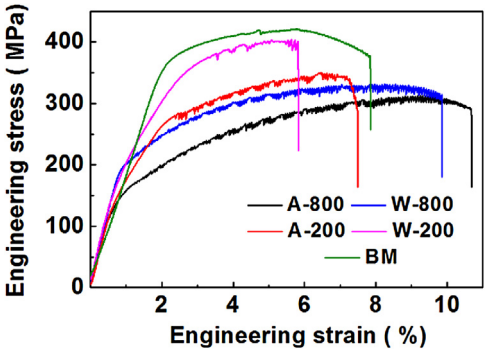

Fig. 7. Engineering tensile stress-strain curves of the FSW joints under various parameters.

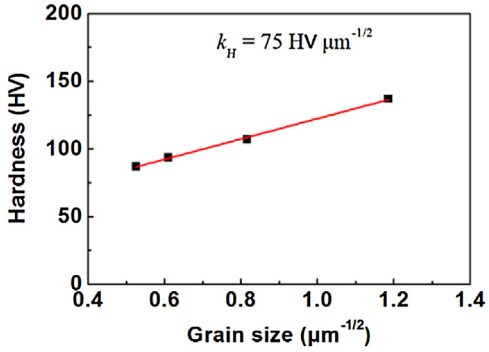

Fig. 6. Relationship between Vickers hardness and average grain size in the NZs of various FSW joints.

rolling. Under a high rotation rate of 800 rpm, a wide lowest hardness zone (LHZ) with uniform hardness values of about 85 HV was observed in the A-800 sample. The width of the LHZ was about 12 mm which was much larger than the width of the NZ (~4.2 mm) in Fig. 1(a). This indicates that significant softening was achieved in the A-800 sample due to the high heat input, and the LHZ consisted of NZ, TMAZ and HAZ. Similar hardness distribution was obtained in the W-800 sample, but the width of the LHZ was slightly reduced to about 10 mm and the lowest hardness value increased to about 90 HV.

As the rotation rate decreased to 200 rpm, the hardness distribution exhibited the typical "W" shape in FSW joints of Al alloys [1,3], and higher hardness value was obtained in the NZ with a width of about 5 mm which was similar to the width of the NZ in Fig. 1(b and d). For the A-200 sample, the LHZ was located at the two sides of the NZ, with the lowest hardness value of 95 HV which was slightly higher than that of the W-800 sample. Compared to the A-800 and W-800 samples, the average hardness value significantly increased to about 105 HV in the NZ of the A-200 sample.

Under rapid water cooling at a very low rotation rate of 200 rpm, the hardness value further increased in the NZ. The average hardness value in the NZ of the W-200 sample was about 137 HV, which was even higher than that of the BM. Similar to the A-200 sample, the W-200 sample also exhibited two narrow LHZs at the two sides of the NZ, i.e. at the HAZ. However, the lowest hardness value significantly increased to about 116 HV for the W-200 sample, which reached about 91% of the BM. This indicates that almost no softening occurred in the HAZ, which should be attributed to the significantly decreased peak temperature and duration time at high temperature [19].

Fig. 6 shows the relationship between the average grain size and the hardness value in the NZ of various samples. Clearly, the hardness value (HV) increased with decreasing grain size (d), and they followed the Hall-Petch relationship:

$$\mathrm{HV} = H_0 + k_{\mathrm{H}} d^{-1/2} \quad (1)$$

where H_0 and k_{H} are constants associated with the hardness measurements. Therefore, the significantly enhanced hardness value in the NZ of the W-200 sample should be mainly attributed to the much refined grain size. Larger Hall-Petch slope (k_{H}) of 75 HV $\mu m^{-1/2}$ was obtained in this study compared to other FSW studies [35,36], which was originated from the relatively higher dislocation densities in the NZs under water cooling and low rotation rate [37].

The engineering tensile stress-strain curves of the FSW joints under different parameters are shown in Fig. 7. It can be seen from the stress-strain curves that the serrated flow was observed in all FSW joints, which was consistent with the results of other researchers [35,38]. For the A-800, W-800 and A-200 samples, serrated flow appeared after the yielding and high serration intensity was observed at larger strain. It is well accepted that clouds of Mg solute atoms create a drag force which hinder the movement of dislocations at a certain strain rate, resulting in the serrated flow phenomenon. However, the serrated flow was not clear in the BM and W-200 sample due to the initial high dislocation density.

The tensile properties of the BM and various FSW joints are shown in Table 1, and all the FSW joints failed at the LHZ during the tensile tests. Very high YS of 370 MPa and UTS of 425 MPa together with a relatively low elongation of 5.7% were achieved in the BM, attributable to severe work hardening. Under a high rotation rate of 800 rpm, the YS and UTS of the A-800 sample significantly decreased to 150 MPa and 314 MPa, respectively, with an increased elongation of 9.2% due to the significantly softening in the wide LHZ. By applying water cooling, the YS and UTS slightly increased to 210 MPa and 328 MPa, respectively, and a similar elongation of 8.4% was achieved in the W-800 sample.

Compared to the A-800 sample, the YS and UTS increased to 260 MPa and 344 MPa in the A-200 sample, respectively. However, the elongation decreased to 4.8% due to the local plastic deformation in the narrowed HAZ. When applying additional water cooling, the YS further increased to 340 MPa in the W-200 sample, which was similar to that of the BM. Similarly, the UTS increased to 403 MPa, resulting in a very high joint coefficient of 95%. The elongation decreased to only 3.5% due to the serious local deformation in the narrow HAZ.

From the above results, it is clear that the joint coefficient was about 74% for normal FSW joint (A-800), which was similar to the result of Peel et al. (the joint coefficient was 67%) [9]. By the combination of low rotation rate and additional water cooling, nearly equal strength to the BM was obtained in the W-200 sample. Previous study indicated that the peak temperature was only 130 °C

in the HAZ of FSW Cu joint at a low rotation rate of 400 rpm with water cooling [19]. Therefore, almost no softening was achieved in the HAZ of the present W-200 sample, resulting in the greatly enhanced mechanical properties.

Obviously, the present study demonstrates that high property FSW joints for severe work-hardened BM can be achieved by the combination of low rotation rate and additional rapid water cooling. Under this very low heat input condition, the softened region was eliminated or extremely suppressed, and the mechanical properties were improved greatly. Therefore, this study provides an effective method of achieving high property FSW joints of work-hardened and precipitate-hardened Al alloys.

4. Conclusions

1. Defect-free FSW joints of 5083Al-H19 alloy were achieved at 800 and 200 rpm with and without additional water cooling. Fine and ultrafine equiaxed grains were obtained in the NZs, and the dislocation density decreased clearly compared to that of the BM.
2. An obvious LHZ was observed from the hardness distribution of A-800 sample. By applying the water cooling, the LHZ was narrowed and the lowest hardness value increased in the W-800 sample. While the rotation rate decreased to 200 rpm, the hardness value increased clearly in the NZ, and even larger than that of the BM in the W-200 sample.
3. The BM exhibited a very high UTS of 425 MPa, and the joint coefficient was only 74% for the normal FSW joint (A-800). High property joint with nearly equal strength to the BM was achieved in the W-200 sample due to the significantly reduced softening.

Acknowledgments

This work was supported by the National Natural Science Foundation of China under grant Nos. 51301178 and 51331008.

References

[1] R.S. Mishra, Z.Y. Ma, Mater. Sci. Eng. R 50 (2005) 1–78.
[2] P.L. Threadgill, A.J. Leonard, H.R. Shercliff, P.J. Withers, Int. Mater. Rev. 54 (2009) 49–93.
[3] R. Nandan, T. Debroy, H. Bhadeshia, Prog. Mater. Sci. 53 (2008) 980–1023.
[4] Y. Yue, Z. Li, S. Ji, Y. Huang, Z. Zhou, J. Mater. Sci. Technol. 32 (2016) 671–675.
[5] P. Cavaliere, M. Cabibbo, F. Panella, A. Squillace, Mater. Des. 30 (2009) 3622–3631.
[6] L. Wan, Y. Huang, W. Guo, S. Lv, J. Feng, J. Mater. Sci. Technol. 30 (2014) 1243–1250.
[7] Y. Birol, S. Kasman, Mater. Sci. Technol. 29 (2013) 1354–1362.
[8] H. Lombard, D.G. Hattingh, A. Steuwer, M.N. James, Eng. Fract. Mech. 75 (2008) 341–354.
[9] M. Peel, A. Steuwer, M. Preuss, P.J. Withers, Acta Mater. 51 (2003) 4791–4801.
[10] Z. Zhang, B.L. Xiao, D. Wang, Z.Y. Ma, Metall. Mater. Trans. A 42 (2010) 1717–1726.
[11] Q. Wang, Z. Zhao, Y. Zhao, K. Yan, H. Zhang, Mater. Des. 88 (2015) 1366–1376.
[12] H.J. Liu, H.J. Zhang, L. Yu, Mater. Des. 32 (2011) 1548–1553.
[13] F. Khodabakhshi, A.P. Gerlich, A. Simchi, A.H. Kokabi, Mater. Sci. Eng. A 620 (2015) 471–482.
[14] C. Sharma, D.K. Dwivedi, P. Kumar, Mater. Sci. Eng. A 556 (2012) 479–487.
[15] P. Xue, B.L. Xiao, Z.Y. Ma, J. Mater. Sci. Technol. 29 (2013) 1111–1115.
[16] P. Xue, Z.Y. Ma, Y. Komizo, H. Fujii, Mater. Lett. 162 (2016) 161–164.
[17] Z. Zhang, B.L. Xiao, Z.Y. Ma, Mater. Charact. 106 (2015) 255–265.
[18] H.J. Zhang, H.J. Liu, Mater. Des. 45 (2013) 206–211.
[19] P. Xue, B.L. Xiao, Q. Zhang, Z.Y. Ma, Scr. Mater. 64 (2011) 1051–1054.
[20] P. Xue, W.D. Li, D. Wang, W.G. Wang, B.L. Xiao, Z.Y. Ma, Mater. Sci. Eng. A 670 (2016) 153–158.
[21] N.T. Kumbhar, S.K. Sahoo, I. Samajdar, G.K. Dey, K. Bhanumurthy, Mater. Des. 32 (2011) 1657–1666.
[22] A.L. Etter, T. Baudin, N. Fredj, R. Penelle, Mater. Sci. Eng. A 445–446 (2007) 94–99.
[23] W.F. Xu, J.H. Liu, D.L. Chen, G.H. Luan, J.S. Yao, Mater. Sci. Eng. A 548 (2016) 89–98.
[24] P. Xue, B.B. Wang, F.F. Chen, W.G. Wang, B.L. Xiao, Z.Y. Ma, Mater. Charact. 121 (2016) 187–194.
[25] Q.Z. Wang, Z.X. Zhao, Y. Zhao, K. Yan, C. Liu, H. Zhang, Mater. Des. 102 (2016) 91–99.
[26] P. Xue, Z.Y. Huang, B.B. Wang, Y.Z. Tian, W.G. Wang, B.L. Xiao, Z.Y. Ma, Sci. China Mater. 59 (2016) 531–537.
[27] S. Rouhi, A. Mostafapour, M. Ashjari, Sci. Technol. Weld. Join. 21 (2016) 41–49.
[28] Z.Y. Ma, A.L. Pilchak, M.C. Juhas, J.C. Williams, Scr. Mater. 58 (2008) 361–366.
[29] F.C. Liu, Z.Y. Ma, Metall Mater. Trans. A 39 (2008) 2378–2388.
[30] K. Osamura, T. Ogura, Metall. Trans. A 15 (1984) 835–842.
[31] R. Goswami, G. Spanos, P.S. Pao, R.L. Holtz, Metall. Mater. Trans. A 42 (2010) 348–355.
[32] D. Singh, P.N. Rao, R. Jayaganthan, Mater. Des. 50 (2013) 646–655.
[33] D. Kim, H. Badarinarayan, J.H. Kim, C. Kim, K. Okamoto, R.H. Wagoner, K. Chung, Eur. J. Mech. A 29 (2010) 204–215.
[34] K. Chen, W. Gan, K. Okamoto, K. Chung, R.H. Wagoner, Metall. Mater. Trans. A 42 (2010) 488–507.
[35] G.R. Cui, Z.Y. Ma, S.X. Li, Acta Mater. 57 (2009) 5718–5729.
[36] Y.S. Sato, M. Urata, H. Kokawa, K. Ikeda, Mater. Sci. Eng. A 354 (2003) 298–305.
[37] Y. Ito, N. Tsuji, Y. Saito, H. Utsunomiya, T. Sakai, J. Jpn. Inst. Met. 64 (2000) 429.
[38] I. Charit, R.S. Mishra, J. Mater. Res. 19 (2004) 3329–3342.